논 문
58-3-22

# 레이저 디스플레이를 위한 전자력 구동 스캐닝 미러의 설계

# Design of Electromagnetically Driven Micro Scanning Mirror for Laser Animation System

이 경 건* · 장 윤 호** · 유 병 욱*** · 진 주 영*** · 임 용 근§ · 김 용 권†
(Kyoung Gun Lee · Yun-Ho Jang · Byung-Wook Yoo · Joo-Young Jin · Yonggeun Lim · Yong-Kweon Kim)

**Abstract** - In this paper, we present the design of an electromagnetic scanning mirror with torsional springs. The scanning mirror consisting of torsional springs and electromagnetic coils was designed for the applications of laser animation systems. We analyzed and optimized three types of torsional springs, namely, straight beam springs (SBS), classic serpentine springs (CSS), and rotated serpentine springs (RSS). The torsional springs were analyzed in terms of electrical resistance, fabrication error tolerance, and resonance mode separation of each type using analytical formula or numerical analysis. The RSS has advantages over the others as follows: 1) A low resistance of conductors, 2) wide resonance mode separation, 3) strong fabrication error tolerance, 4) a small footprint. The double-layer coils were chosen instead of single-layer coils with respect to electromagnetic forces. It resulted in lower power consumption. The geometry of the scanning mirror was optimized by calculations; RSS turn was 12 and the width of double-layer coil was 100 ㎛, respectively. When the static rotational angle is 5 degrees, the power consumption of the mirror plate was calculated to be 9.35 mW since the resistance of the coil part and a current is 122 Ω and 8.75 mA, respectively. The power consumption of full device including the mirror plate and torsional springs was calculated to be 9.63 mW.

**Key Words** : Laser animation system, Scanning mirror, Serpentine spring, Electromagnetic coil

## 1. Introduction

Since 1980s, scanning mirrors using MEMS technology have been studied and developed intensively in the applications including imaging systems [1], scanning devices [2-7], and high power laser systems. The mirror structures including mechanical flexures and their driving mechanisms are different to fit the application requirements, but torsional springs are usually adopted for rotational mirrors.

The torsional spring is related with resonant frequency and mechanical torque. The straight beam springs (SBS) are most commonly used in scanning mirrors due to structural simplicity [8-10]. The SBS, however, should be long to achieve the same amount of torsional angle in a large mirror. The long SBS has a couple of drawbacks such as a small ratio of resonant frequencies along z-axis to a resonant frequency of rotation, and a large lateral length. Serpentine springs including classic serpentine springs (CSS) and rotated serpentine springs (RSS) have been numerically analyzed to alleviate the problems of the SBS [11]. The selection of spring types and its optimization should start from the design specifications and be analyzed based on resonant frequencies and fabrication error tolerance.

Electrostatic actuations, piezoelectric actuations, and electromagnetic actuations are popularly used for driving mechanisms for scanning mirrors. An electrostatic actuation is a preferred method due to its simplicity, but the angular deflection is generally limited by the gap between driving electrodes. Since a driving voltage of the electrostatic actuator increases in proportional to the square of the gap between electrodes, the voltage should be large to obtain large angular deflections. On the contrary, an electromagnetic actuation is preferred in the applications of large angular deflections, since it has a large driving force compared with the electrostatic actuations.

In this paper, we present the design of an electromagnetic scanning mirror supported with torsional springs. The design factors are as follows: Serpentine torsional springs and electromagnetic coils. Three types of

* 준 회 원 : 서울대학교 전기·컴퓨터 공학부 석사과정
** 정 회 원 : 서울대학교 전기·컴퓨터 공학부 연구교수
*** 정 회 원 : 서울대학교 전기·컴퓨터 공학부 박사과정
§ 비 회 원 : 한국 알엠아이 (주)
† 교신저자, 시니어회원 : 서울대학교 전기·컴퓨터 공학부 교수
E-mail : yongkkim@snu.ac.kr
접수일자 : 2009년 1월 29일
최종완료 : 2009년 2월 9일

torsional springs including SBS, CSS, and RSS are analyzed and compared to optimize springs under the requirements of the scanning mirror. The electromagnetic coils under a mirror plate is optimized in terms with power consumption.

## 2. Design specifications

Laser animation systems could draw random patterns on walls, ceilings or other surfaces. Fig. 1 shows the schematic of the laser animation system consisting of a laser light source, a two axis scanning mirror driven by an electromagnetic force, and permanent magnets for generating magnetic field. The laser source has a wavelength of 625 nm and a spot size of 2.0 mm diameter. A mirror plate reflects the laser beam into the display area both vertically and horizontally. The maximum mechanical tilting angle should be larger than 5 degrees since the display area is 2 m × 2 m and the distance to the screen is 11 m.

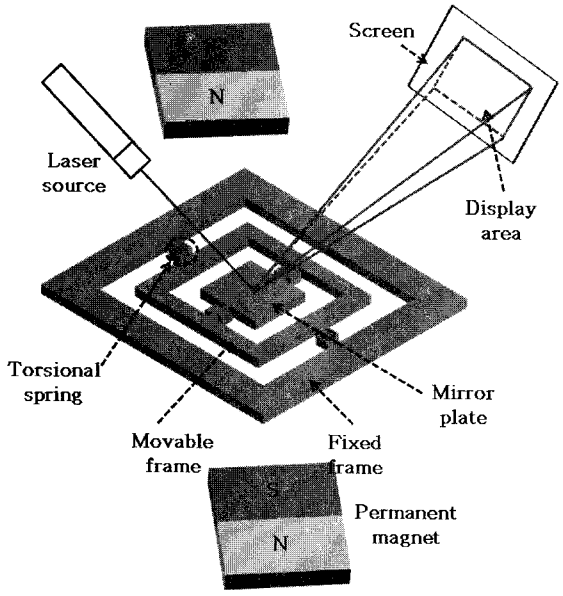


**Fig. 1** Schematic view of the laser animation system

Fig. 2. shows the detailed rotation principle of the mirror plate and the movable frame. A current flowing inside a spiral coil induces the Lorentz force in the 45 degree tilted magnetic field. In this system, the only single magnet pair is used to generate magnetic field for both the mirror plate and the movable frame. The tilted magnetic field is decomposed into two orthogonal directions, and the only magnetic field perpendicular to the current direction can influence the electromagnetic operation. The Lorentz force on different edges from a rotation axis is generated same direction torque, even though in a single magnet pair.

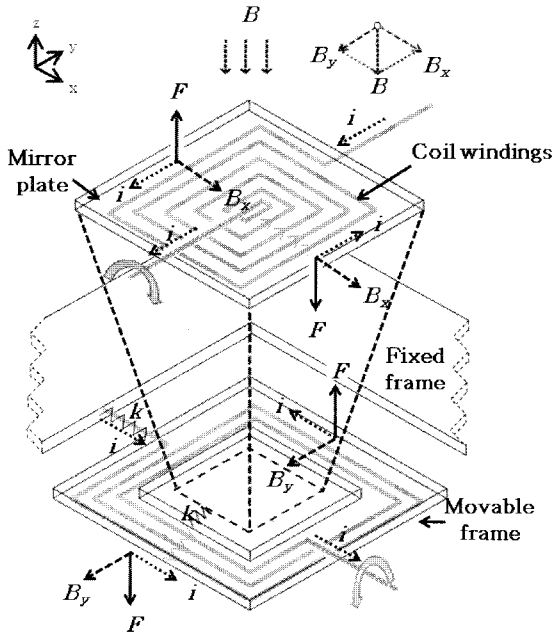


**Fig. 2** Rotation principle of the scanning mirror

The size of the mirror plate should be 2.5 mm × 2.5 mm to reflect the 2.0 mm diameter laser. The thickness of the structural layer is set to be 50 ㎛ due to the fabrication process. The lateral length of torsional spring is limited by 500 ㎛ to minimize a chip size. The resonant frequency of the scanning mirror should be larger than 400 Hz since the scanning mirror will operate actuate in vector scan mode. The laser animation system requires relatively large angular deflections with in DC signals.

## 3. Design of torsional springs

Three types of torsional springs are shown in Fig. 3. Giuseppe Barillaro *et al.* derived stiffness equations under the assumption of slender beam approximations, where a beam thickness is relatively smaller than the width and the length of the beam. The result of equation based on the slender beam approximations shows more 10 % error than finite element method (FEM) calculations, because spring dimensions are different from the assumptions of beam approximations [11]. Therefore, FEM simulation (COMSOL Multiphysics 3.4) is used to analyze resonant frequencies instead of analytic equations using beam approximations. Table 1 shows simulated model parameters and results of resonant frequency. Firstly, we set the resonant frequency to be around 400 Hz. Then, the dimensions of six springs from three types are extracted by FEM simulations to fit the resonant frequency. The serpentine spring turns, the parallel length and orthogonal length of the spring are calculation

parameters. The scanning mirror has two pairs of springs to suspend a mirror plate and a movable frame. This chapter describes the design procedure for a pair of springs in a mirror plate, but it can be easily expanded into a movable frame.

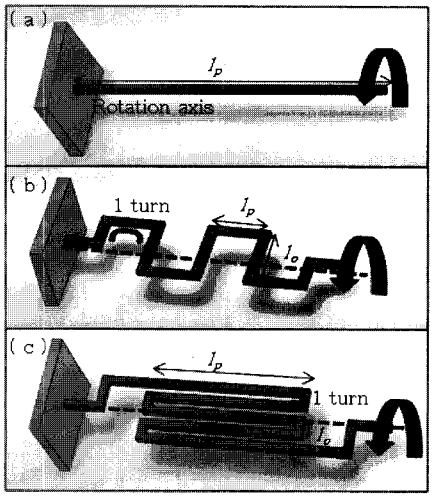


**Fig. 3** Structural views of three spring types. (a) Straight beam spring (SBS), (b) classic serpentine spring with 4 turns (CSS) and (c) rotated serpentine spring with 4 turns (RSS).

**Table 1** Simulated parameters and result of resonant frequency

| Parameter | Spring models | | | | | |
|---|---|---|---|---|---|---|
| | SBS | CSS | | RSS | | |
| Spring turns (N) | | 4 | 12 | 4 | 12 | 22 |
| Parallel length $l_p$ ($\mu$m) | 4250 | 100 | 100 | 600 | 220 | 90 |
| Orthogonal length $l_o$ ($\mu$m) | | 1200 | 350 | 70 | 70 | 70 |
| Torsional resonant frequency $f_\theta$ (Hz) | 401 | 408 | 405 | 393 | 403 | 413 |

### 3.1 Spring length effect on resistance

The coil width on springs are naturally limited by the spring width, while the coil width on the mirror plate can be optimized. The length of coils on springs are small, but the is small enough to affect total resistance of the coil.

The specific resistance, $\rho$, and the thickness of coils, $t$ are measured to be 0.0036 $\Omega\mu$m and 0.85 $\mu$m, respectively. The resistance of spring coils on springs, $r$, is calculated by the equation,

$$r = \rho \frac{l}{t \times w} \quad (1)$$

, where $l$ is the conductor length and $w$ is conductor width.

Table 2 shows the calculation results of coil on springs in case that all springs have the approximately same spring stiffness as well as the approximately same resonant frequencies. The CSS shows larger resistance than that of other models, which means the CSS is longer than other models. The RSS with 4 turns shows the lowest resistance 1.6 Ω.

**Table 2** Summarized spring analysis

| Parameter | Spring models | | | | | |
|---|---|---|---|---|---|---|
| | SBS | CSS | | RSS | | |
| Spring turns (N) | | 4 | 12 | 4 | 12 | 22 |
| Resistance on springs(Ω) | 1.8 | 2.3 | 2.4 | 1.6 | 1.9 | 2.3 |
| Resonant frequency ratio, $f_z/f_\theta$ | 1.3 | 3.4 | 3.2 | 5.3 | 4.6 | 2.9 |
| Maximum frequency variation (%) | -23.7 | -23 | -22.5 | -17.6 | -20.1 | -22 |
| Lateral length ($\mu$m) | 4250 | 600 | 1400 | 860 | 480 | 350 |

### 3.2 Resonance mode separation

Fig. 4 shows two resonance modes of one axis mirror. The first mode (Fig. 4(a)) is a torsional actuation and the second mode (Fig. 4(b)) is z-axis actuation. If two modal frequencies are close, unwanted actuation will easily occur.

It is important to put the undesired frequencies as far as possible for stable operations. Table 2 also shows the simulation results of resonance mode separation defined as the first and the second frequency ratios, $f_z$ divided by $f_\theta$, as an index of stability. A high frequency ratio means a high stability. While the SBS shows the lowest resonant frequency ratio, the RSS with lower turns shows wide mode separation. The resonance mode separation of the RSS becomes worse as spring turns increase.

### 3.3 Fabrication error tolerance

The strong tolerance against fabrication errors is generally important for uniform characteristics such as the resonant frequency. The resonant frequency of the scanning mirror is designed to be 400 Hz. Since the mirror will actuate around 300 Hz at maximum in a static mode, over 25% resonant frequency variation may

cause resonance. Therefore, resonant frequency variation should suppressed under 25 % after fabrication.

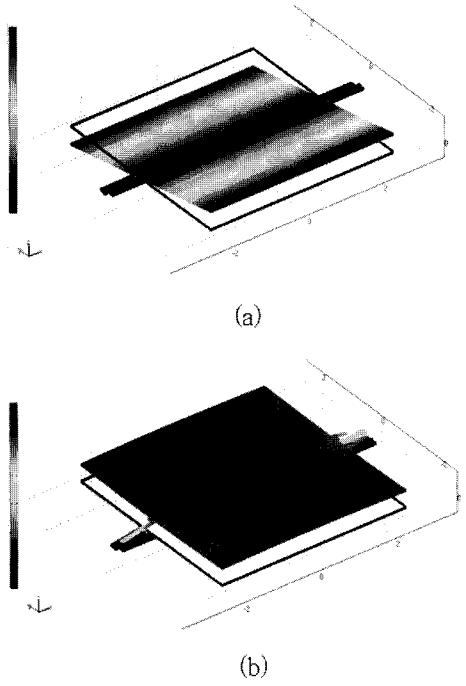


**Fig. 4** Example of modal views of (a) the first resonance mode (fΘ), (b) the second resonance mode (fz)

The fabrication process is described briefly as shown in Fig. 5. The metal layer is deposited and lifted off on the insulation layer from the top side of an silicon on oxide( SOI) wafer (Fig. 5(a)). Then, additional insulator and second metal layer is formed to complete electromagnetic coils (Fig. 5(b)). Torsional springs and mirror patterns are formed on the device layer, and then whole structures are released from the backside by silicon etching (Fig. 5(c), (d)).

There are two major fabrication error possibilities in the process. First, a spring thickness is easily varied from the design due to the footing effect in deep reactive ion etching (DRIE) process. A thickness variation of the SOI wafer can also be a factor for the thickness variation. Second, a spring width are caused by the undercut effect during the DRIE process and photolithography. The thickness error is much larger than width error through the fabrication process. Therefore, the thickness variation more than width variations are selected as follows : ±10 , ±20 % of 50 ㎛ thickness and 4, 2, -2, -4, -6, -8 % of 50 ㎛ width.

A resonant frequency variation is plotted and listed in Fig. 6 associated with the deviated frequency divided by the initial frequency. As shown in Fig. 6(a), the resonant frequency of the RSS has smaller errors than that of the CSS in terms of a thickness error.

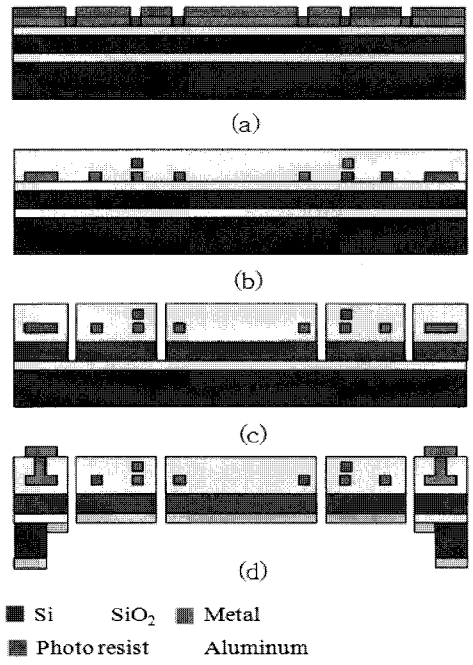


**Fig. 5** Fabrication process. (a) 1st photolithography and metal deposition, (b) after metal lift-off and $SiO_2$ deposition, 2nd metal lift-off and $SiO_2$ deposition, (c) deep reactive ion etching (DRIE) patterning, (d) backside DRIE patterning and aluminum deposition.

On the contrary, a width error gives more significant effect on the RSS than the CSS as shown in Fig. 6(b). To find the maximum variation of resonant frequency, the worst cases of thickness and width errors are calculated together as shown in Fig. 7. Three cases of the RSS show better tolerance than other types. The RSS with 12 turns has 20.1 % variation when the thickness error and the width error are -20 % and -8 %, respectively. Note that the increasing coil turns reduce a lateral chip size but the resonant frequency becomes more sensitive to fabrication errors.

## 4. Design of electromagnetic coils

There are many types of electromagnetic coils for various applications [1, 4, 10]. Especially, an electromagnetic coil with a single-layer (Fig. 8 (a)) is usually adopted in many scanning mirrors because of its simplicity [12]. But multi-layer coils can achieve stronger magnetic flux than the single-layer coil [10].

Both single and double-layer coils are considered in terms of power consumption. We also optimize the width of the double-layer coils for minimum power consumption because the laser animation system allows under 20 mW power consumption. The analysis is done for the coils on the mirror part without coils on springs.

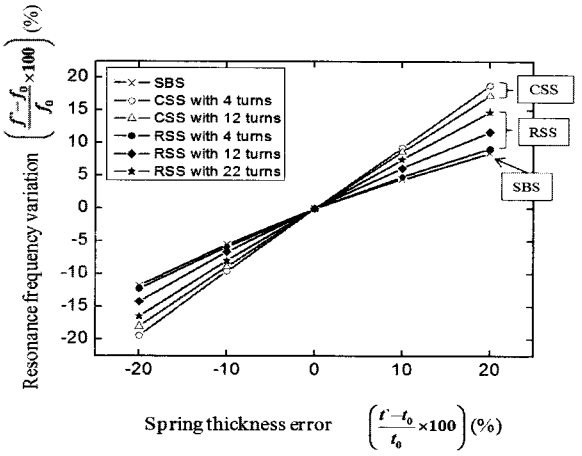


| Thickness error (%) | Resonant frequency variation (%) | | | | | |
|---|---|---|---|---|---|---|
| | SBS | CSS | | RSS | | |
| | | 4 | 12 | 4 | 12 | 22 |
| -20 | -11.7 | -19.4 | -18.0 | -12.2 | -14.1 | -16.5 |
| -10 | -5.5 | -9.6 | -8.9 | -5.9 | -6.6 | -8.0 |
| 0 | 0.0 | 0.0 | 0.0 | 0.0 | 0.0 | 0.0 |
| 10 | 4.5 | 9.3 | 8.6 | 4.8 | 6.2 | 7.5 |
| 20 | 8.5 | 18.9 | 17.3 | 9.2 | 11.7 | 14.8 |

(a)

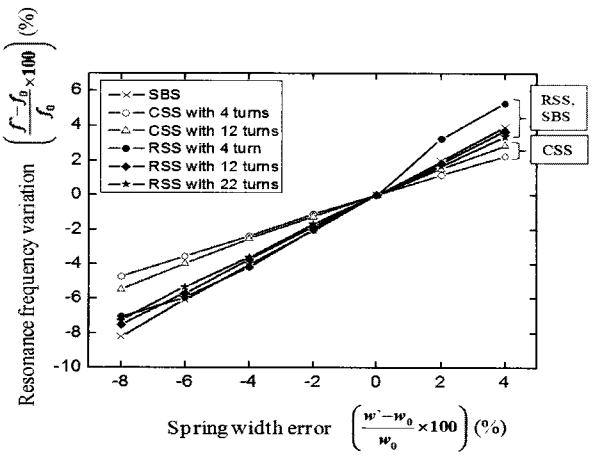


| Width error (%) | Resonant frequency variation (%) | | | | | |
|---|---|---|---|---|---|---|
| | SBS | CSS | | RSS | | |
| | | 4 | 12 | 4 | 12 | 22 |
| -8 | -8.2 | -4.7 | -5.5 | -7.0 | -7.5 | -7.3 |
| -6 | -6.1 | -3.6 | -4.0 | -6.0 | -5.7 | -5.3 |
| -4 | -4.1 | -2.4 | -2.5 | -4.2 | -3.7 | -3.6 |
| -2 | -2.1 | -1.1 | -1.3 | -2.0 | -1.9 | -1.7 |
| 0 | 0.0 | 0.0 | 0.0 | 0.0 | 0.0 | 0.0 |
| 2 | 2.0 | 1.2 | 1.5 | 3.3 | 1.9 | 1.7 |

(b)

**Fig. 6** Resonant frequency variation according to (a) a spring thickness and (b) a spring width error.

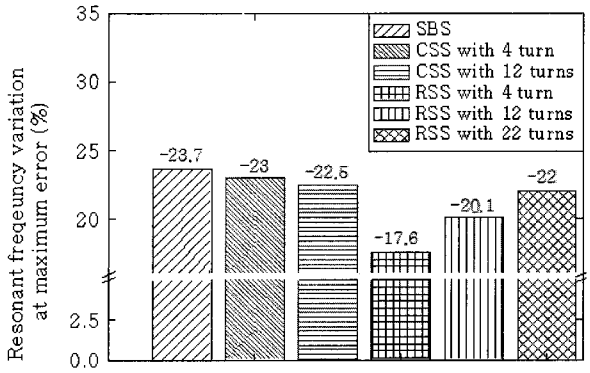


**Fig. 7** Resonant frequency variation at maximum error.

### 4.1 Structure of electromagnetic coils

Electromagnetic coils are usually composed of three parts as shown in Fig. 8. The first layer has spiral metal coils on an insulating material. The contact via electrically connects the first layer to the second layer for current carrying.

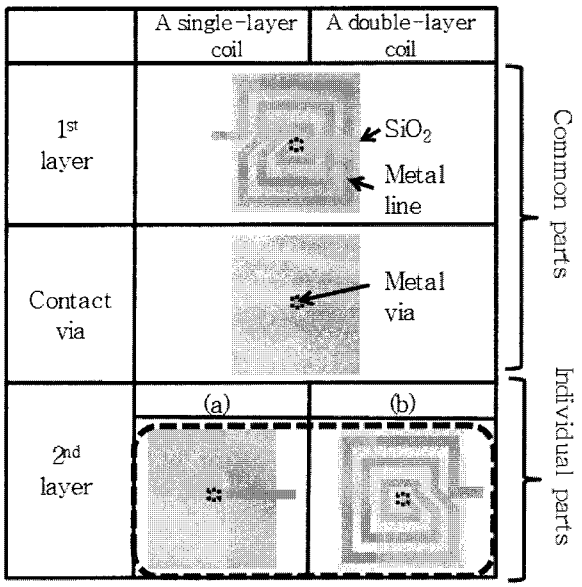


**Fig. 8** Schematic views of (a) a single-layer coil and (b) a double-layer coil.

As shown in Fig. 8(a), the second layer of the single-layer coil connects mirror part coils to spring part coils. The second layer of the double-layer coil in Fig. 8(b) has additional coils. The second layer coil requires no extra fabrication processes but just changing a layout. The double-layer coil can manipulate twice force as much as the single-layer coil with the same current so that less power consumption by two times for the same deflection angle is expected.

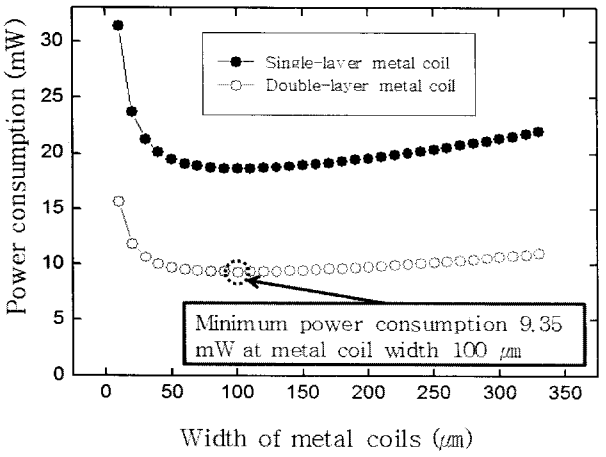


**Fig. 9** The coil width effect of the single and double-layer coils on power consumption

### 4.2 Optimization of power consumption

Additional coils on the second layer have influence on resistances, currents, voltages, and power consumption. We calculated the power consumption of the double-layer coils with various widths to find out an optimal value for minimum power consumption.

The space gap between coil windings are designed as 10 ㎛ for prevention from current leakage and misalignment. The resistance coil, $R$, is given by the following equation,

$$R = \rho \frac{1}{wt} \sum_k l_k \tag{2}$$

, where $l_k$ is the length of unit conductor and $k$ is the winding turn number of the coil. The current, $I$, is extracted from the equilibrium condition between an electromagnetic torque by the coil and a mechanical torque by torsional springs.

$$\left| \sum_k (\vec{B} \times \vec{l_k} I) \times \vec{r_k} \right| = k_\theta \theta \tag{3}$$

$$I = \frac{k_\theta \theta}{\left| \sum_k (\vec{B} \times \vec{l_k}) \times \vec{r_k} \right|} \tag{4}$$

, where $k_\theta$ is the stiffness of the torsional spring, $\theta$ is the torsional angle, $B$ is the magnetic field of 0.3 T, $r_k$ is the distance between a rotation axis of the mirror and the current carrying conductor. The stiffness of the torsional spring is obtained from the resonant frequency. The power consumption, $P$, for a certain torsional angle is then calculated by Ohm's law using Eq. (2) and (4), and it is expressed as,

$$P = I^2 R = \left| \frac{k_\theta \theta}{\sum_k (\vec{B} \times \vec{l_k}) \times \vec{r_k}} \right|^2 \left( \rho \frac{1}{wt} \sum_k l_k \right) \tag{5}$$

Eq. (5) shows a relationship between the coil width and the power consumption so that the optimal width can be obtained from the numerical calculation. As shown in Fig. 9, double-layer coils give half power consumption compared with the single-layer coil. Minimum power consumption of 9.35 mW appears at 100 ㎛ width and 11 coil turns. The resistance of the coil and the current are calculated as 122 Ω, 8.75 mA, respectively.

### 5. Result of scanning mirror design

Table 3 shows the selected parameters for the current application based on the analysis. At first, the RSS has better performance than the other types so that we have chosen the RSS as the torsional springs for the current application.

**Table 3** Result of the design and expected performance

| Design result | |
|---|---|
| Torsional spring | |
| Parallel length, $l_p$ (㎛)<br>Orthogonal length, $l_o$ (㎛) | 220 ㎛, 70 ㎛ |
| Spring turns ($N$) | 12 |
| Electromagnetic coil | |
| Coil width | 100 ㎛ |
| Space between coil windings | 10 ㎛ |
| Spiral coil turns | 11 |
| Expected performance | |
| Resonant frequency, $f_\theta$ | 403 Hz |
| Resistance of the coil on springs | 1.9 Ω × 2 |
| Resonant frequency ratio, $f_\theta$ / $fz$ | 4.6 |
| Lateral length | 480 ㎛ |
| *Power consumption of the coil under the mirror plate only | 9.35 mW |
| Power consumption of the coil of the full device | 9.63 mW |
| *Metal line in mirror plate | 122 Ω |
| *Current | 8.75 mA |

*Only the mirror plate is biased

While small turns of the RSS show better results except the lateral length as shown in Table 1, the RSS with 12 turns has been selected because the lateral length of the device should be smaller than 500 ㎛. The selected spring have a parallel length of 220 ㎛ and an orthogonal length of 70 ㎛, which results in the lateral length of 480 ㎛. The optimized coil width using the double-layer spiral is 100 ㎛ and space between windings is 10 ㎛. Using this designed parameters, the resonant frequency is calculated to be 403 Hz and electrical resistance on springs is 3.8 Ω. The resonant frequency separation between 1st and 2nd modes is 4.6. The designed double-layer coil will have 122 Ω and the required current for 5 degree actuation is 8.75 mA. The expected power consumption of coils under only the mirror plate

and the full device including coils on springs are 9.35 mW and 9.63 mW, respectively.

## 6. Conclusion

We described an approach to design an electromagnetic scanning mirror with torsional springs. The SBS, CSS, and RSS were analyzed by FEM simulation and calculation. The RSS with 12 turns was adopted to the scanning mirror because it has various advantages such as low resistance, small dependency on the spring thickness variation, and wide separation between the first and the second resonant frequencies. The double-layer coils were expected to consume half lower power than single-layer coils. Also a width of the metal coils was optimized for minimal power consumption of 9.35 mW and 9.63 mW for the mirror plate and the full device, respectively. The designed scanning mirror could be applied to a laser animation system.

## References


[1] Arda D. Yalcinkaya, Hakan Urey, Dean Brown, Tom Montague, and Randy Sprague, "Two-axis electromagnetic Microscanner for High Resolution Displays", Journal of Microelectromechanical Systems, vol. 15, no. 4, pp. 786-794, 2006.

[2] L. O. S. Ferreira and S. Moehlecke, "A silicon micromechanical galvanometric scanner", Sensors and Actuators A, Physical, vol. 73, pp. 252-260, 1999.

[3] Hiroshi Toshiyoshi, Wibool Piyawattanametha, Cheng-Ta Chan, and Ming C. Wu, "Linearization of electrostatically actuated surface micromachined 2-D optical scanner," Journal of Microelectromechanical Systems, vol. 10, pp. 205-214, 2001.

[4] Takayuki Fujita, Kazusuke Maenaka, Yoichiro Takayama, "Dual-axis MEMS mirror for large deflection-angle using SU-8 soft torsion beam", Sensors and Actuators A, Physical, vol. 121, pp. 16-21, 2005.

[5] D. Wine, M. P. Helsel, L. Jenkins, H. Urey, and T. D. Osborn, "Performance of a bi-axial MEMS-based scanner for microdisplay applications," in Proceedings of SPIE, vol. 4178, pp. 186-196, 2000.

[6] Reyne Gilbert, "Electromagnetic actuation for MOEMS, examples, advantages and drawbacks of MAGMAS", Journal of Magnetism and Magnetic Materials, vol. 242-245, pp. 1119-1125, 2002.

[7] Si-Hong Ahn and Yong-Kweon Kim, "Silicon scanning mirror of two DOF with compensation current routing", Journal of Micromechanics and Microengineering, vol. 14, pp. 1455-1461, 2004.

[8] Yun-Ho Jang, Kook-Nyung Lee and Yong-Kweon Kim, "Characterization of a single crystal silicon micromirror array for maskless UV lithography in biochip applications", Journal of Micromechanics and Microengineering, vol. 16, pp. 2360-2368, 2006.

[9] Eric Leclerc, Alexis Debray, Nicolas Tiercelin, Teruo Fujii, and Hiroyuki Fujita, "Silicon based optical scanner using PDMS as torsion springs," in Proceedings of Optical MEMS, pp.95-96, 2003.

[10] D. Niarchos, "Magnetic MEMS : Key issues and some applications," Sensors and Actuators A, Physical, vol. 109, pp. 166-173, 2003.

[11] Giuseppe Barillaro, Antonio Molfese, Andrea Nannini and Francesco Pieri, "Analysis, simulation and relative performances of two kinds of serpentine springs", Journal of Micromechanics and Microengineering, vol. 15, pp. 736-746, 2005.

[12] Hiroshi Miyajima, Nobuyoshi Asaoka, Toshihiko Isokawa, Masanori Ogata, Yukihiro Aoki, Masaharu Imai, Osamu Fujimori, Masahiro Katashiro, and Kazuya Matsumoto, "A MEMS electromagnetic optical scanner for a commercial confocal laser scanning microscope," Journal of Microelectromechanical Systems, vol. 12, no. 3, pp. 243-251, 2003.


## 저 자 소 개


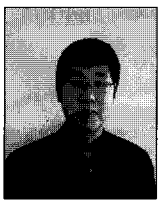

**이 경 건 (李 炅 鍵)**

2008년 서울대학교 전기 컴퓨터 공학부 졸업. 2008년~ 현재 동대학원 석사 과정
E-mail : leekgun1@snu.ac.kr

**장 윤 호 (張 潤 虎)**

1999년 서울대학교 전기컴퓨터 공학부 졸업. 2001년 동대학원 전기컴퓨터 공학부 졸업 (석사). 2005년 동대학원 전기컴퓨터 공학부 졸업 (박사). 2005년~2008년 삼성 전자 책임연구원. 2008년~현재 서울대학교 전기·컴퓨터 공학부 BK 연구교수.
E-mai : yunhojang@snu.ac.kr

**유 병 욱 (兪 炳 旭)**

2005년 서울대학교 전기·컴퓨터 공학부 졸업. 2007년 동대학원 석사 졸업. 2007년~현재 동대학원 박사 과정.

E-mail : despina1@snu.ac.kr

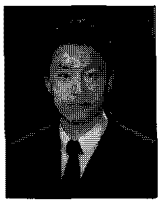

**진 주 영 (陳 周 暎)**

2003년 고려대학교 전기·전자·전파공학부 졸업. 2009년 서울대학교 대학원 전기·컴퓨터 공학부 졸업(석사). 2009년~현재 서울대학교 대학원 전기·컴퓨터 공학부 박사과정.

E-mail : damugi@snu.ac.kr

**임 용 근 (任 容 槿)**

1990년 한양대학교 자연·과학대학 물리학과 졸업. 1992년 동대학원 물리학과 졸업(석사). 1994년~2002년 (주)대우전자 TMA 사업부 모듈개발팀; 선임 연구원. 2002년~2005년 (주)오카스 부설 연구소 연구소장. 2006년~현재 (주)한국 알엠아이 연구소장

E-mail : yonggeun.lim@rmikorea.com

**김 용 권 (金 容 權)**

1983년 서울대학교 전기공학과 졸업. 1983년 동대학교 대학원 전기공학과 졸업 (석사). 1990년 동경대학교 대학원 졸업 (박사). 1990년~1992년 히타치 중앙연구소 연구원. 1992년~현재 서울대학교 전기·컴퓨터 공학부 교수.

E-mail : yongkkim@snu.ac.kr